Results in Physics 42 (2022) 106008

Contents lists available at ScienceDirect

Results in Physics

journal homepage: www.elsevier.com/locate/rinp

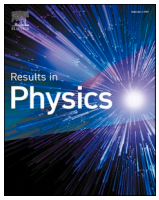

Acoustic edge mode in spiral-based metamaterials at subwavelength scale

Tao Yang [a,b], Boya Xiao [a,b], Yafei Feng [c], Dongliang Pei [a,b], Yu Liu [a,b], Meng Chen [a,b,*], Heng Jiang [a,b,*], Zhongyu Zheng [a,b], Yuren Wang [a,b]

[a] Key Laboratory of Microgravity, Institute of Mechanics, Chinese Academy of Sciences, Beijing 100190, People's Republic of China
[b] University of Chinese Academy of Sciences, Beijing 100049, People's Republic of China
[c] Units 92228 of Chinese People's Liberation Army, Beijing 100072, People's Republic of China

ARTICLE INFO

Keywords:
Spiral structure
Subwavelength
Topological phononic crystal

ABSTRACT

Recently, the quantum effect of condensed matter physics is introduced into the acoustic field, which lays a new pathway to manipulate the acoustic wave. However, the acoustic topological insulator based on Bragg scattering requires their lattice constant to be comparable with the wavelength. In this paper, a novel subwavelength spiral element on the basis of the Archimedean spiral is proposed. Thanks to the central resonator with a slender curved channels scheme, the subwavelength Dirac cone forms in the band structure. The eigenfrequency of the element can be changed by the spiral geometric parameters, which triggers the topological phase transition characterized by opposite valley Chern numbers. The backscattering-immune unidirectional transmission edge state exists at different topological boundaries, suggesting its great robustness even at the sharp bends. Also the topological edge modes along the Z-shaped interfaces are verified by the experiments and the calculation, which provides an effective structure to control the low frequency acoustic wave transmission.

Introduction

The discovery of the quantum Hall effect [1,2], quantum spin Hall effect [3,4], and quantum Valley Hall effect [5,6] have promoted the development of condensed matter physics, which attracts much attention on the topological insulator. One of its most unique properties is the backscattering-immune unidirectional transmission. The electrons could travel along the edges or surfaces smoothly despite of defects. These characteristics have inspired the classical realms [7–12]. However, the classical wave systems belong to the boson system, and don't have the spin effect that is unique to the electronic system. Moreover, there is no such external field analogue to the magnetic field in acoustics to break the time inversion symmetry. It is quite challenging to realize quantum effects in acoustic systems.

At the early stage, Fleury et al. [10] break the time inversion symmetry in acoustics by introducing the circulating fluid, which splits the resonant ring cavity's azimuthal resonant modes resulting in the analogue "Zeeman Effect". Armed with this principle, several designs [13,14] of analogue quantum Hall effect in acoustics have been realized. Later, the researchers [15,16] implemented the Floquet topological insulators based on space–time modulation and waveguide coupling. Although the acoustic pseudospin can be artificially realized by the above methods, these structures are quite complex and require harsh external conditions. Therefore, in view of the time protected quantum spin Hall effect and quantum Valley Hall effect, researchers [17–20] construct acoustic topological insulator with specific symmetry using simple units and break the space-reversal symmetry through changing the geometric parameters, so as to achieve the analogue quantum effect without harsh external conditions. In contrast, this method is more practical and simpler. However, this kind of acoustic topological insulators is equipped with inversion symmetry when constructing the unit cell. On the other hand, the size of phononic crystal element is equivalent to the acoustic wavelength. These harsh requirements restrict the design of the acoustic topological valley system. Thus, it is desirable to introduce the subwavelength structural units with lower symmetry to realize the one-way transmission edge state in low-frequency in order to effectively control the low-frequency sound waves. Notably, some effective strategies [21–23] have been reported to deal with this challenge in realizing acoustic transitions and boundary states at subwavelength scales. However, these strategies are only suitable for surface acoustic waves (SAW), which are not effective for waveguide acoustic waves (WAW). Though space-folding structure [24,25] and Helmholtz resonator [26,27] have been introduced into the topological acoustic system, these schemes make the system complex.

* Corresponding authors at: Key Laboratory of Microgravity, Institute of Mechanics, Chinese Academy of Sciences, Beijing 100190, People's Republic of China.
E-mail addresses: chenmeng@imech.ac.cn (M. Chen), hengjiang@imech.ac.cn (H. Jiang).

https://doi.org/10.1016/j.rinp.2022.106008
Received 21 July 2022; Received in revised form 30 August 2022; Accepted 19 September 2022
Available online 21 September 2022

Lately, spiral and chiral unit cells [28–30] have been applied in the construction of metamaterials. They own a variety of geometric parameters such as chirality, rotation angle, and spiral width, which show fruitful control on acoustic waves like double negative characteristics and abnormal acoustic beam. Furthermore, this kind of structures enjoys the chiral scheme, shares the subwavelength characteristics and is simple to construct. Thus, they would be a better option for subwavelength topological structure and exhibit abundant possibilities to realize topological phase transition due to its fruitful geometric parameters. Although the topological insulators with chiral and spiral structure have been recently reported a little study focus on the subwavelength characteristics. Here we propose a novel subwavelength chiral structure taking inspiration from the spiral and chiral elements.

It is noted that there are a large share of spiral structures controlled by distinct parameters. In order to simplify the unit cell design, we construct a unique spiral unit cell based on the Archimedean spiral structure owing to its simple mathematical form. In addition, it enjoys a chiral scheme, the inversion symmetry is not necessary when constructing the unit cell. Then, the local resonance effect is introduced into the unit cell trying to lower its eigenfrequency by constructing a resonator at the center of the unit cell. Moreover, six slender curved channels joined in the resonator reduce the eigenfrequency further thanks to the space-folding scheme. Because the slender curved channels bend the air channels, and the length of the sound path has been extended, which gives rise to higher refractive index and causes lower eigenfrequency. Thus, a subwavelength Dirac cone [31–34] formed at the K, K' point in the energy band. The lattice symmetry can be lowered by altering the two adjacent spiral units' outer radius, which leads to topological phase transition characterized by opposite Valley Chern numbers. Finally, the robustness of topological edge modes transmitting along the interfaces containing two sharp bends is verified by the experiment and simulation.

Structure design and method

The Archimedean spiral structure is shown in Fig. 1 (a). The spiral equation is$r(s) = R-(R-r)s, \phi(s) = 2\pi ns$, where R is the outer radius of the Archimedean spiral ($R = 1.2$ cm), r is the inner radius of the Archimedean spiral ($r = 0.8$ cm), n is the number of turns of the spiral,$s \in [0; 1]$, and w is the width of the spiral ($w = 1$ mm). Select a section of the Archimedes spiral ($n = 0.3$) and rotate it anticlockwise around the center of the spiral. The same spiral section is obtained every 60 degrees, and then these spirals are combined together to form a spiral phononic crystal unit. The unit cell is illustrated in Fig. 1 (b). The whole spiral unit is embedded as a scatterer in the honeycomb unit cell matrix filled with air. The honeycomb lattice with spiral units is to be considered as C_6 symmetry, marked by the red dashed line in Fig. 1(c). The lattice constant is $a = 5$ cm. The adjacent spiral unit cells highlighted with colored orange and blue are marked by A and B, respectively.

Employing the finite-element software COMSOL Multiphysics to calculate the energy band structure of the spiral metamaterials. Since the spiral is made of epoxy ($c_0 = 2540m/s$, $\rho_0 = 1100kg/m^3$), its impedance is greater than that of air ($c_0 = 343m/s$, $\rho_0 = 1.29kg/m^3$), the spiral can be regarded as the rigid scatterer. At the same time, in order to simplify the calculation model, Floquet Bloch boundary conditions are applied to the opposite side of the honeycomb lattice, so that only one lattice element is necessary to be calculated. Along the boundary of the first Brillouin zone, M - Γ - K-M scanning wave vector is adopted to obtain the energy band structure of the whole phononic crystal. The band structure is shown in Fig. 2 (a), since the phononic crystals have C_6 symmetry, and the K-point carries C_3 symmetry, there exists a deterministic Dirac cone [35] at the K point of the Brillouin zone at 2345 Hz, with its normalized frequency $f_n = 0.342$ ($f_n = f \cdot a/c$, c is the sound velocity in air, 343 m/s). Because the spiral lattice element can be considered to be a central resonator with six slender curved channels, the local resonance effect is introduced into the unit cell trying to lower its eigenfrequency by constructing a resonator at the center of the unit

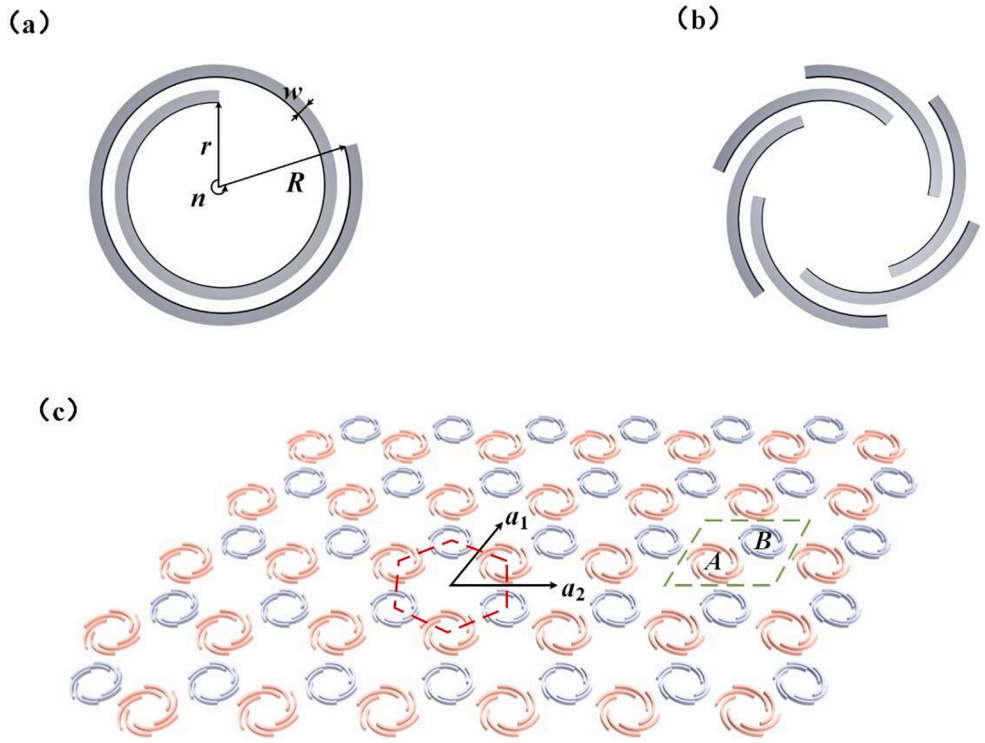

Fig. 1. (a) An Archimedes spiral with its geometric parameters. (b) Schematic illustration of the spiral unit cell. (c) Topological phononic crystal is composed of spiral unit cells distributed in a honeycomb lattice. The adjacent spiral unit cells highlighted with colored orange and blue are marked by A and B, respectively. (For interpretation of the references to colour in this figure legend, the reader is referred to the web version of this article.)

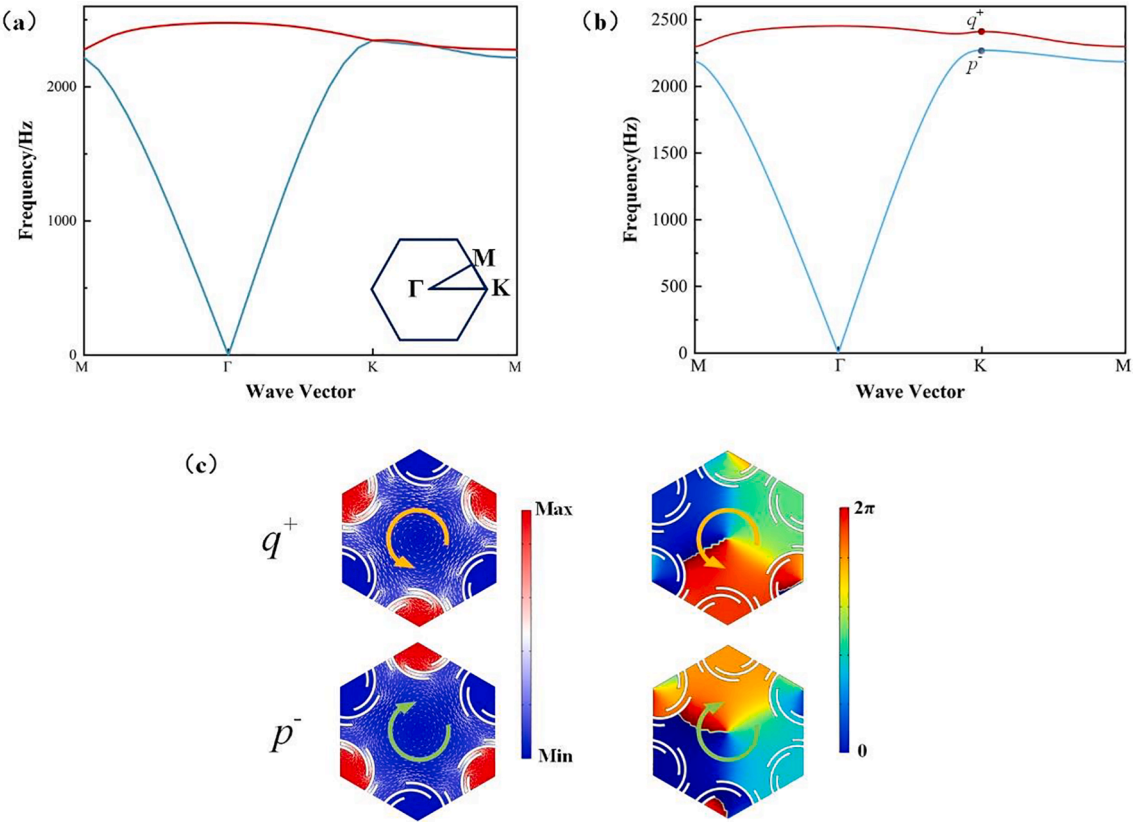

Fig. 2. (a) The band structure of the spiral phononic crystal with $t = 0$ cm. (b) The band structure of the spiral phononic crystals with $t = 0.03$ cm. (c) The amplitude and phase distributions for eigenstates q^+ and p^-. The green and yellow arrows stand for the interior vortex field with clockwise and counter-clockwise directions, respectively. (For interpretation of the references to colour in this figure legend, the reader is referred to the web version of this article.)

cell. Moreover, six slender curved channels joined in the resonator reduce the eigenfrequency further thanks to the space-folding scheme. The combined action of these two compositions contributes to the subwavelength Dirac cone.

Since the subwavelength Dirac cone is formed, we can focus on opening a topological band gap and tailoring the topological properties of the system. Then the inversion symmetry can be broken by changing the geometric parameters of the adjacent units. Here we choose to adjust the outer radius R of the spiral. The outer radius of unit cell A is increased by t (t = 0.03 cm), and the outer radius of unit cell B is decreased by t. The adjacent units A and B with different outer radius are no longer symmetrical, and the symmetry of the whole crystal structure is reduced to C_3 symmetry. Then, the energy band structure after changing the geometric parameters is calculated, and the calculation results are shown in Fig. 2 (b). It can be found that when the geometric parameters of the structure change, the scheme of the unit cell A and B also changes, resulting in different eigenfrequencies between them. The Dirac cone at the K point splits, giving rise to two eigenstates q^+ (2370 Hz) and p^- (2324 Hz), forming a band gap. The amplitude and phase distributions of the eigenstates q^+ and p^- are shown in Fig. 2(c). The interior energy flow in eigenstate q^+ enjoys a clockwise direction, which is consistent with the direction of the phase. As for the eigenstate p^-, it enjoys a counter-clockwise direction of the interior energy flow and phase. Thus, these two eigenstates share opposite chirality.

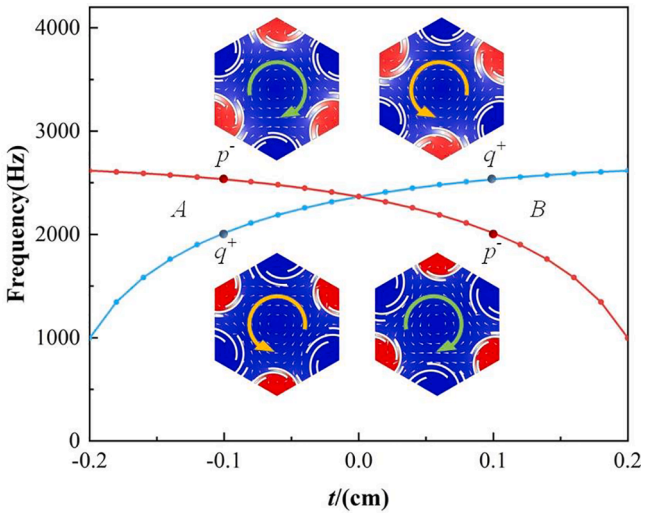

Fig. 3. The frequency of q^+ and p^- states at K point in Brillouin zone as a function of t. The green and yellow arrows stand for the interior vortex field with clockwise and counter-clockwise directions, respectively. (For interpretation of the references to colour in this figure legend, the reader is referred to the web version of this article.)

Results and discussion

Topological phase transition

Fig. 3 shows a continuous evolution of the band-edge frequencies q^+ and p^- versus the spiral outer radius variation t. When $t = 0$, the two adjacent spiral units are in the same geometric scheme and share the same eigenfrequency, and there exists a Dirac cone at the K point of the first Brillouin zone. As the value of t gradually deviates from $t = 0$, the degeneracy at the K point is lifted and the subwavelength band gap forms. To demonstrate the process of the topological phase transition clearly, the eigenstates q^+, p^- at t = -0.1 cm and $t = 0.1$ cm are shown in

Fig. 3. At the left side of $t = 0$, the eigenstate p^- is located at the upper boundary of the subwavelength band gap with a clockwise interior vortex field, while the eigenstate q^+ state is located at the lower boundary of the subwavelength band gap with a counter clockwise interior vortex field; For the right side of $t = 0$, eigenstates p^- and q^+ exchange their positions of the upper and lower boundary of the band gap. Evidently, it can be found that during the process of t changing, the frequency order of the first two bands is inverted at $t = 0$, locked to the opposite vortex pseudospins. Thus, a topological protected unidirectional transmission boundary state can form at the boundary.

According to the *k-p* perturbation method, the effective Hamiltonian is constructed [11]:

$$\delta H = v_D \delta k_x \sigma_x + v_D \delta k_y \sigma_y + m v_D^2 \sigma_z \quad (1)$$

Where v_D is the Dirac velocity at the Dirac cone, $\delta k = (\delta k_x, \delta k_y)$ is the momentum deviation from the K point, and σ_i are the Pauli matrices. The effective mass can be characterized by:

$$m = (\omega_{q^+} - \omega_{p^-})/2v_D^2 \quad (2)$$

Since the effective mass relies on the frequency of the two eigenstates p^- and q^+ the effective Hamiltonian is linked strongly to t. The Valley Chern number can be derived by integrating the local Berry curvature $\Omega(\delta k)$ centered at the K point:

$$C_K = \frac{1}{2\pi}\int \Omega(\delta k) dS = \frac{1}{2} sgn(m) \quad (3)$$

For the domain A, $m < 0$, the Chern number of the second band is $-\frac{1}{2}$ at the K point. For the domain B, $m > 0$, the Chern number of the second band is $\frac{1}{2}$ at the K point.

For the domain A and B, the Chern number shares opposite signs, which confirms the topological phase transition. Thus, the interfaces constructed by two different Valley Hall phases promise the existence of the edge modes.

Edge modes

In order to prove the existence of topological edge modes at the interfaces between domains that enjoy opposite Valley Chern numbers, we construct a ribbon-shaped supercell, as shown in Fig. 4 (a). The supercell is composed of two types of phononic crystals, labeled with type-I ($t =$ 0.1 cm) and type-II ($t = -0.1$ cm). Type-II phononic crystal with a length of $10a$ is located in the middle of the supercell whereas type-I phononic crystal with a length of $8a$ is located at the end of the supercell, which forms a sandwich structure. There exist two types of interfaces in this supercell, interface I-II and interface II-I, denoted with M and N, respectively. In calculation, apply the periodic boundary condition to the left and right sides of the supercell and exert the perfectly matched layer on the upper and lower boundary of the supercell. Thus, the band structure of the supercell is obtained.

Fig. 4(b) shows the band structure of the sandwich supercell. The black solid line indicates the bulk state, red and blue solid lines indicate the edge modes at interface N and M respectively. They show different slopes, which indicate opposite group velocity. Points M_R, M_L, N_R, and N_L stand for the edge modes propagating towards left and right on the interfaces M and N. Edge modes M_R and N_R are situated in the band gap with the wavenumber$k_x = \frac{\pi}{2a}$, and edge modes M_L and N_L are situated in the band gap with the wavenumber$k_x = \frac{3\pi}{2a}$. Fig. 5 displays the pressure field and energy flow distribution on the interfaces M and N for these four edge modes (M_R, M_L, N_R, N_L). It reveals that quite a few of the energy is concentrated on the interface, indicating the edge modes. Also, according to the direction of energy flow, the edge modes travel in one direction at the interface, which is consistent with the direction of wavenumber. The edge modes of supercell are labeled as M_R, M_L, N_R, and N_L respectively. L and R represent the left and right directions of propagation, while M and N represent two types of interfaces. For example, M_L means acoustic waves transmit to the left at the interface M, N_R means acoustic waves transmit to the right at the interface N. The helix edge modes at the interfaces show that it is similar to the electronic system's valley pseudospin.

Then, we designed a straight waveguide and a Z-shaped waveguide in a $16a \times 22a$ superlattice consisted of type-I ($t = 0.1$ cm) and type-II ($t = -0.1$ cm) spiral units, as shown in Fig. 6(a) and Fig. 6(b), respectively. When the point source located at the left side of the waveguide is excited at 2100 Hz, the sound waves transmit along the waveguide from the left side to the right side smoothly. Even for the Z-shaped waveguide where exist two sharp bends in the transmission path, the sound waves still transmit along the waveguide smoothly, shown in Fig. 6(b). The simulated sound pressure distribution verifies the existence of the edge mode and shows its robust transmission.

To demonstrate the backscattering suppression of topological transmission around the sharp corner, we have derived transient intensity fields in Z-shaped waveguide. In Fig. 7(a), a Z-shaped waveguide is constructed, marked by the blue dashed line. A Gaussian burst pulse

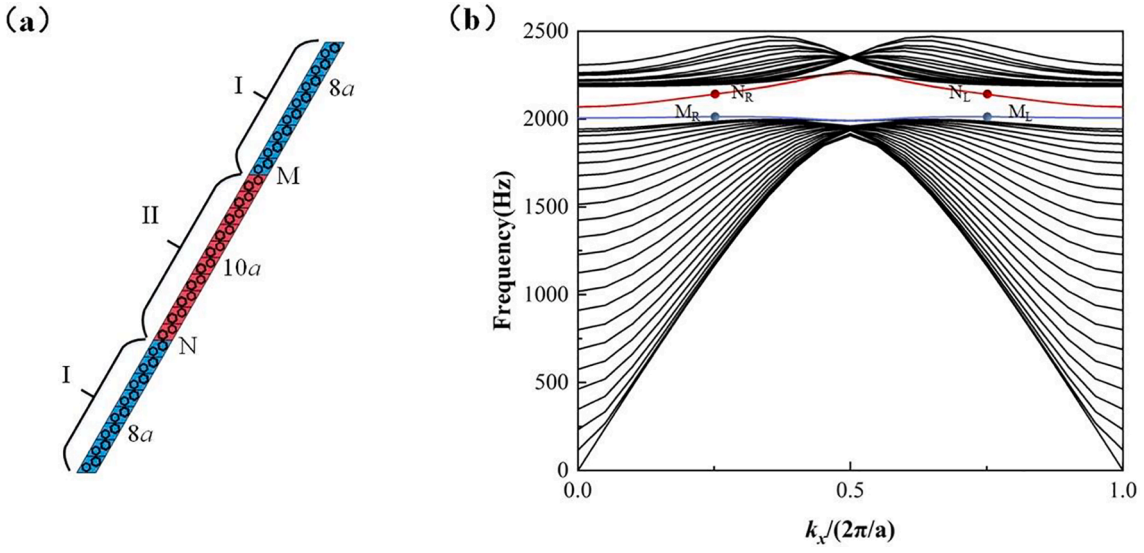

Fig. 4. (a) The ribbon-shaped superlattice consisted of type-I and type-II phononic crystals. (b) The band structure of the supercell, points M_R, M_L, N_R, and N_L stand for the edge state with specific momentum at the interfaces N and M.

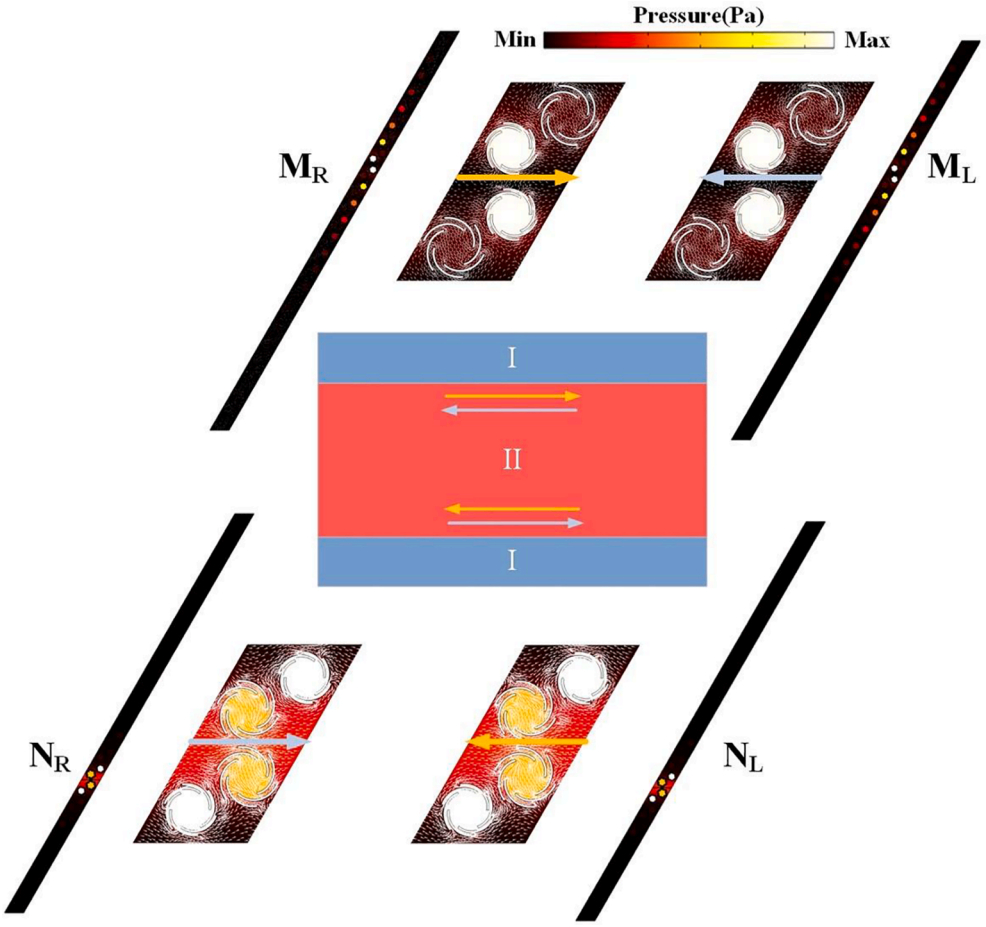

Fig. 5. The real-space distributions of the pressure and intensity field on the interfaces M and N for the four eigenstates. The yellow and white arrows stand for the energy flow in right and left directions, respectively. (For interpretation of the references to colour in this figure legend, the reader is referred to the web version of this article.)

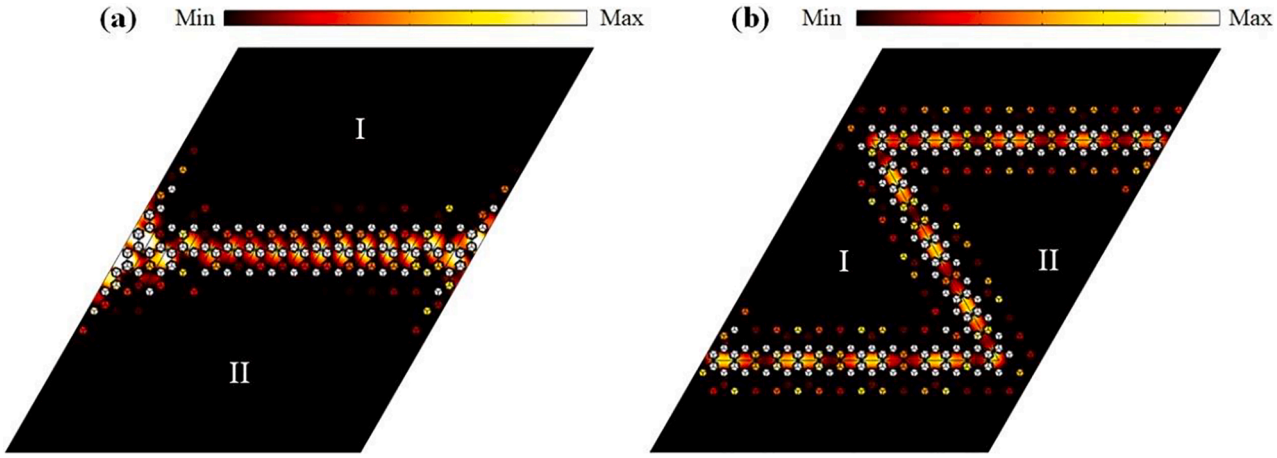

Fig. 6. Simulated sound pressure distributions of (a) Straight waveguide and (b) Z-shaped waveguide at 2100 Hz.

with six cycles at $f = 2112$ Hz is excited at the left side of the waveguide. The transient intensity fields in Z-shaped waveguide at four different times (t = 0.03 s, 0.05 s, 0.064 s, and 0.09 s) are shown in Fig. 7(b). It suggests that the sound waves propagate along the waveguide smoothly. The time history of sound pressure at point B and C (shown in Fig. 7(c)) reveals that the amplitude of the sound waves is almost the same before and after transmitting the two sharp corners. It presents the backscattering suppression merits of the edge states.

Experiment

So as to verify the robust transmission of the edge modes, we construct a Z-shaped waveguide in a finite $16a \times 22a$ superlattice. The sample made of epoxy is fabricated by a 3D printer, as shown in Fig. 8 (a). In the diagram, the blue dashed line indicates the Z-shaped topological interfaces. In the experiment, the spiral metamaterials covered with a plexiglass plate are placed on the epoxy base plate, where the

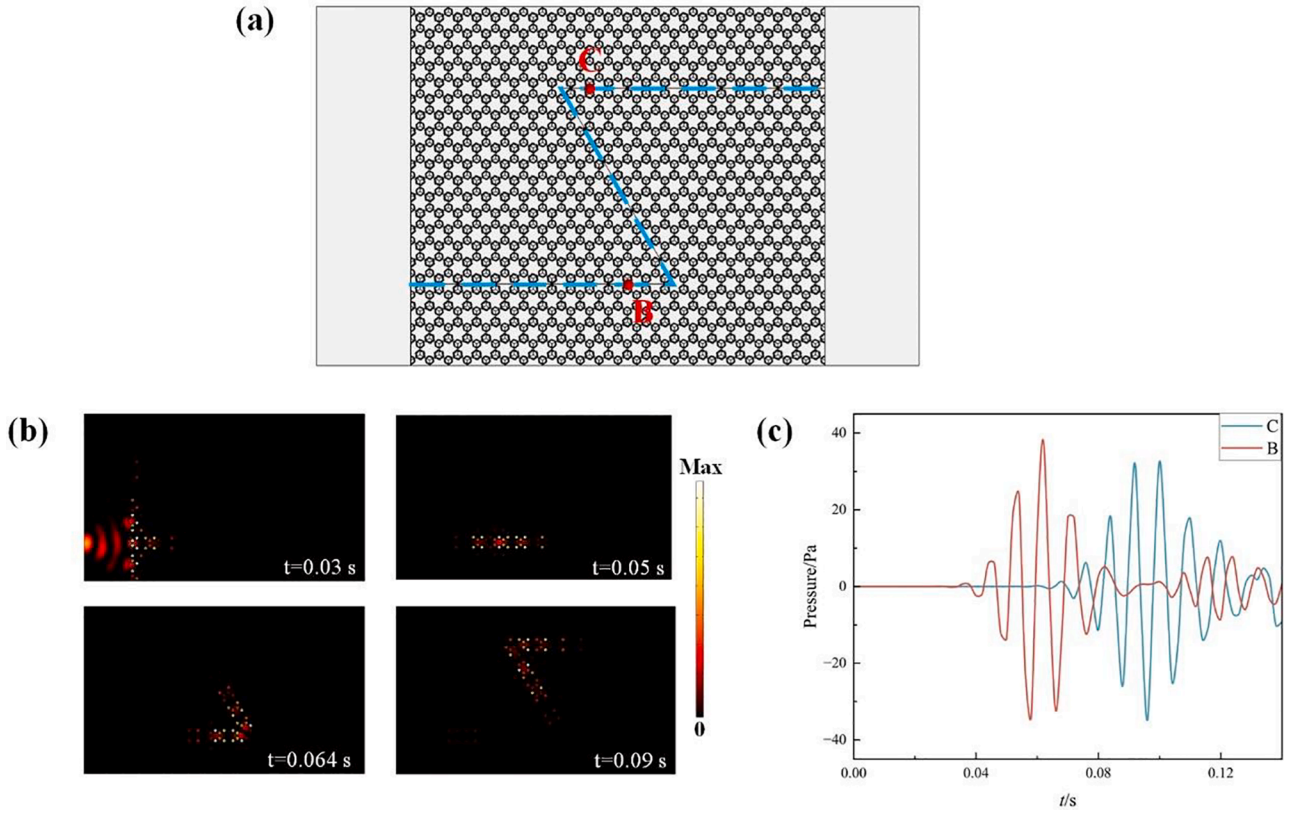

Fig. 7. (a) Demonstration of the Z-shaped waveguide. (b) The transient intensity fields in Z-shaped waveguide at four different times (t = 0.03 s, 0.05 s, 0.064 s, and 0.09 s). (c) Time history of sound pressure at points B and C.

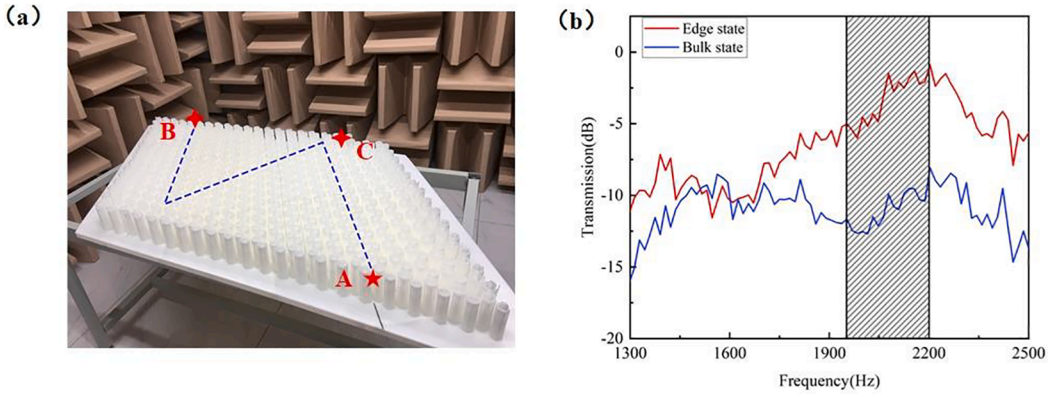

Fig. 8. (a) Photograph of a fabricated Z-shaped waveguide sample. Point A stands for the sound wave input port, and points B and C stand for the measuring end for edge state and bulk state, respectively. (b) Experimentally measured transmission spectra of topological edge states and bulk states.

experiment is regarded to be undertaken in a 2D waveguide. For the sake of minimizing the effect of the reflection wave, the entire experiment is conducted in the anechoic room and the upper and lower boundaries are filled with sound absorbing cotton. The speaker (BOACH-BLS-55) as a point source is placed at port A. Then, the white noise ranging from 1300 Hz to 2500 Hz is excited from the point source. The sound intensity signals at ports B and C are collected by a 1/4-inch microphone (BSWA-MPA-201), which denote edge state and bulk state, respectively. The collected sound intensity signals are transferred to the PC to post process through the data acquisition card (NI-9234). Fig. 8(b) illustrates the transmission spectra of acoustic waves through the Z-shaped superlattice. The edge state and bulk state are denoted by the red and blue solid lines, respectively. In the frequency range of the band gap denoted by the shaded area, the acoustic waves transmit mainly in the form of edge modes since the transmission of edge state is ~10 dB higher than the bulk state. Thus, in the topological band gap, there exist edge modes in the Z-shaped channel, which verifies the simulation results.

Conclusions

In this paper, we construct a novel subwavelength spiral unit cell based on Archimedes' spiral structure, which can be equivalent to a central resonator with six slender curved channels. This unit cell lowers the whole system eigenfrequency on the grounds of the local resonance effect and space folding scheme. Distribute the unit cell in the honeycomb lattice with C_6 structure symmetry, which produces a subwavelength Dirac cone in the energy band at 2345 Hz, with normalized frequency $f_n = 0.342$. The symmetry of the lattice can be reduced

through altering the two adjacent spiral units' geometric parameters, then the topological band gap forms and the Dirac cone splits into two eigenstates at K point. Furthermore, to demonstrate the process of topological phase transition the sound field distribution of two eigenstates at K point is calculated characterized by opposite Valley Chern numbers. Moreover, the existence of edge modes is verified by the superlattice consisted of opposite Valley Hall phases. Finally, the robust transmission of edge mode is proved by simulations and experimental results, which exhibits the backscattering-immune merits despite of the defects. This kind of subwavelength spiral structure lays a new pathway to manipulate the low-frequency sound waves.

CRediT authorship contribution statement

Tao Yang: Conceptualization, Methodology, Writing – original draft. **Boya Xiao:** Data curation. **Yafei Feng:** Investigation. **Dongliang Pei:** Formal analysis. **Yu Liu:** Validation. **Meng Chen:** Conceptualization. **Heng Jiang:** Writing – review & editing. **Zhongyu Zheng:** Writing – review & editing. **Yuren Wang:** Supervision.

Declaration of Competing Interest

The authors declare that they have no known competing financial interests or personal relationships that could have appeared to influence the work reported in this paper.

Data availability

The data that has been used is confidential.

Acknowledgements

This work is supported by the National Natural Science Foundation of China (Grant No 11972034), the Strategic Priority Research Program of the Chinese Academy of Sciences (Grant No XDB22040301), the Research Program of Beijing (Grant No Z161100002616034), and the Youth Innovation Promotion Association of the Chinese Academy of Science (Grant No 2020018).

Appendix A. Supplementary data

Supplementary data to this article can be found online at https://doi.org/10.1016/j.rinp.2022.106008.

References

[1] Klitzing KV, Dorda G, Pepper M. New Method for High-Accuracy Determination of the Fine-Structure Constant Based on Quantized Hall Resistance. Phys Rev Lett 1980;45:494–7.
[2] Laughlin RB. Anomalous Quantum Hall Effect: An Incompressible Quantum Fluid with Fractionally Charged Excitations. Phys Rev Lett 1983;50:1395–8.
[3] Kane CL, Mele EJ. Quantum Spin Hall Effect in Graphene. Phys Rev Lett 2005;95:226801.
[4] Andrei Bernevig B, Shou-Cheng Zhang TLH. Quantum Spin Hall Effect and Topological Phase Transition in HgTe Quantum Wells. Science 2006;314:1757–61.
[5] Yao W, Xiao D, Niu Q. Valley-dependent optoelectronics from inversion symmetry breaking. Phys Rev B 2008;77:235406.
[6] Ju L, Shi Z, Nair N, Lv Y, Jin C, Velasco J, et al. Topological valley transport at bilayer graphene domain walls. Nature 2015;520:650–5.
[7] Wang Z, Chong Y, Joannopoulos JD, Soljačić M. Observation of unidirectional backscattering-immune topological electromagnetic states. Nature 2009;461:772–5.
[8] Hafezi M, Demler EA, Lukin MD, Taylor JM. Robust optical delay lines with topological protection. Nat Phys 2011;7:907–12.
[9] Skirlo SA, Lu L, Soljačić M. Multimode One-Way Waveguides of Large Chern Numbers. Phys Rev Lett 2014;113:113904.
[10] Fleury R, Sounas DL, Sieck CF, Haberman MR, Alù A. Sound Isolation and Giant Linear Nonreciprocity in a Compact Acoustic Circulator. Science 2014;343:516–9.
[11] Lu J, Qiu C, Ye L, Fan X, Ke M, Zhang F, et al. Observation of topological valley transport of sound in sonic crystals. Nat Phys 2016;13:369–74.
[12] Zhang Z, Wei Q, Cheng Y, Zhang T, Wu D, Liu X. Topological Creation of Acoustic Pseudospin Multipoles in a Flow-Free Symmetry-Broken Metamaterial Lattice. Phys Rev Lett 2017;118:084303.
[13] Yang Z, Gao F, Shi X, Lin X, Gao Z, Chong Y, et al. Topological Acoustics. Phys Rev Lett 2015;114:114301.
[14] Ni X, He C, Sun X-C, Liu X-P, Lu M-H, Feng L, et al. Topologically protected one-way edge mode in networks of acoustic resonators with circulating air flow. New J Phys 2015;17:053016.
[15] Fleury R, Khanikaev AB, Alu A. Floquet topological insulators for sound. Nat Commun 2016;7:11744.
[16] Peng YG, Qin CZ, Zhao DG, Shen YX, Xu XY, Bao M, et al. Experimental demonstration of anomalous Floquet topological insulator for sound. Nat Commun 2016;7:13368.
[17] He C, Ni X, Ge H, Sun X-C, Chen Y-B, Lu M-H, et al. Acoustic topological insulator and robust one-way sound transport. Nat Phys 2016;12:1124–9.
[18] Lu J, Qiu C, Ke M, Liu Z. Valley Vortex States in Sonic Crystals. Phys Rev Lett 2016;116:093901.
[19] Lu J, Qiu C, Deng W, Huang X, Li F, Zhang F, et al. Valley Topological Phases in Bilayer Sonic Crystals. Phys Rev Lett 2018;120:116802.
[20] Zhang Z, Tian Y, Cheng Y, Liu X, Christensen J. Experimental verification of acoustic pseudospin multipoles in a symmetry-broken snowflakelike topological insulator. Phys Rev B 2017;96:241306.
[21] Zhang Z, Long H, Liu C, Shao C, Cheng Y, Liu X, et al. Deep-Subwavelength Holey Acoustic Second-Order Topological Insulators. Adv Mater 2019;31:1904682.
[22] Yves S, Fleury R, Lemoult F, Fink M, Lerosey G. Topological acoustic polaritons: robust sound manipulation at the subwavelength scale. New J Phys 2017;19:075003.
[23] Torrent D, Sánchez-Dehesa J. Acoustic Analogue of Graphene: Observation of Dirac Cones in Acoustic Surface Waves. Phys Rev Lett 2012;108:174301.
[24] Dai H, Qian M, Jiao J, Xia B, Yu D. Subwavelength acoustic topological edge states realized by zone folding and the role of boundaries selection. J Appl Phys 2018;124:175107.
[25] Zhang Z, Cheng Y, Liu X, Christensen J. Subwavelength multiple topological interface states in one-dimensional labyrinthine acoustic metamaterials. Phys Rev B 2019;99:224104.
[26] Wang Y, Dong Y, Zhai S, Ding C, Luo C, Zhao X. Reconfigurable topological transition in acoustic metamaterials. Phys Rev B 2020;102:174107.
[27] Yang Z, Peng Y, Li X, Zou X, Cheng J. Boundary-dependent corner states in topological acoustic resonator array. Appl Phys Lett 2020;117:113501.
[28] Foehr A, Bilal OR, Huber SD, Daraio C. Spiral-Based Phononic Plates: From Wave Beaming to Topological Insulators. Phys Rev Lett 2018;120:205501.
[29] Zhu R, Liu XN, Hu GK, Sun CT, Huang GL. Negative refraction of elastic waves at the deep-subwavelength scale in a single-phase metamaterial. Nat Commun 2014;5:5510.
[30] Li S, Yang J. Topological Transition in Spiral Elastic Valley Metamaterials. Phys Rev Appl 2021;15:014058.
[31] Dai H, Xia B, Yu D. Dirac cones in two-dimensional acoustic metamaterials. J Appl Phys 2017;122:065103.
[32] Yves S, Berthelot T, Fink M, Lerosey G, Lemoult F. Measuring Dirac Cones in a Subwavelength Metamaterial. Phys Rev Lett 2018;121:267601.
[33] Zhang Q, Chen Y, Zhang K, Hu G. Dirac degeneracy and elastic topological valley modes induced by local resonant states. Phys Rev B 2020;101:014101.
[34] Dai H, Jiao J, Xia B, Liu T, Zheng S, Yu D. Observation of topological edge states of acoustic metamaterials at subwavelength scale. J Phys D Appl Phys 2018;51:175302.
[35] Lu J, Qiu C, Xu S, Ye Y, Ke M, Liu Z. Dirac cones in two-dimensional artificial crystals for classical waves. Phys Rev B 2014;89:134302.